MASS AND REDSHIFT DEPENDENCE OF STAR FORMATION IN RELAXED GALAXY CLUSTERS

Rose A. Finn[1,2], Michael L. Balogh[3], Dennis Zaritsky[4], Christopher J. Miller[5], Robert C. Nichol[6]
Draft version February 15, 2008

ABSTRACT

We investigate the star-formation properties of dynamically relaxed galaxy clusters as a function of cluster mass for 308 low-redshift clusters drawn from the Sloan Digital Sky Survey (SDSS) C4 cluster catalog. It is important to establish if cluster star-formation properties have a mass dependence before comparing clusters at different epochs, and here we use cluster velocity dispersion, σ, as a measure of cluster mass. We select clusters with no significant substructure, a subset of the full C4 sample, so that velocity dispersion is an accurate tracer of cluster mass. We find that the total stellar mass, the number of star-forming galaxies, and total star-formation rate scale linearly with the number of member galaxies, with no residual dependence on cluster velocity dispersion. With the mass-dependence of cluster star-formation rates established, we compare the SDSS clusters with a sample of $z \simeq 0.75$ clusters from the literature and find that on average (correcting for the mass growth of clusters between the two redshifts) the total Hα luminosity of the high-redshift clusters is 10 times greater than that of the low-redshift clusters. This can be explained by a decline in the Hα luminosities of individual cluster galaxies by a factor of up to ~ 10 since $z \simeq 0.75$. The magnitude of this evolution is comparable to that of field galaxies over a similar redshift interval, and thus the effect of the cluster environment on the evolution of star-forming galaxies is at most modest. Our results suggest that the physical mechanism driving the evolution of cluster star-formation rates is independent of cluster mass, at least for clusters with velocity dispersion greater than 450 km s^{-1}, and operates over a fairly long timescale such that the star-formation rates of individual galaxies decline by an order of magnitude over ~ 7 billion years.

Subject headings: galaxies: clusters

1. INTRODUCTION

Although the inverse correlation between star-formation rates and galaxy density is well-established (e.g. Balogh et al. 1997; Lewis et al. 2002; Gómez et al. 2003), we do not yet understand whether this is due to the advanced evolution in overdense regions or to a direct physical effect on the star formation capability of galaxies in dense environments. The apparent rapid evolution of galaxies in dense environments (Butcher & Oemler 1984; Dressler et al. 1997; Poggianti et al. 1999) suggests that it may be possible to observe the quenching of star formation in dense regions by exploring clusters over a modest range of redshifts ($0 < z < 1$), though great care must be taken to ensure a fair comparison of clusters (e.g. Nakata et al. 2005; Andreon et al. 2006). This evolution may be partly related to an apparent decrease in the spiral population since $z \sim 1$ and a corresponding increase in the S0 population (e.g. Dressler et al. 1999; Smith et al. 2005; Postman et al. 2005; Moran et al. 2007), yet the cause of the morphology and SFR evolution remains unclear.

We have undertaken a program to directly measure star-formation rates (SFRs) of cluster galaxies over this redshift range, and so far we have been able to demonstrate that star-formation rates of cluster galaxies depend on both redshift and cluster mass (Finn et al. 2004, 2005; Poggianti et al. 2006). However, we have not been able to distinguish mass and evolutionary effects because the high-redshift clusters typically have lower masses than the low-redshift clusters. Furthermore, even clusters of comparable mass and redshift exhibit large scatter in their star-formation properties (possibly suggesting that another property of clusters, such as the intracluster medium density, may play a role; Popesso et al. 2007; Moran et al. 2007). Thus, we need to have large samples of clusters with adequate mass coverage to reliably characterize cluster SFR properties. The large and uniform cluster catalogs selected from the Sloan Digital Sky Survey (SDSS; York et al. 2000) are the best available for investigating the dependence of star-formation rates on cluster mass.

Several groups have studied the environmental dependence of SDSS galaxy properties such as morphology, color, and star-formation rate. Often, environment is characterized in terms of the local density (e.g. Gómez et al. 2003; Blanton et al. 2005; Baldry et al. 2006), and it is generally found that the correlations with local density do not depend strongly on the larger-scale environment (e.g. Balogh et al. 2004; Blanton et al. 2005). An alternative approach is to identify bound systems and look for correlations with system mass, where the latter property is measured from galaxy dynamics (e.g. Goto 2005; Rines et al. 2005), X-ray properties (e.g. Popesso et al. 2007) or via direct comparison to model predictions (Weinmann et al. 2006a). Most of these studies have fo-

[1] Department of Physics, Siena College, 515 Loudon Rd, Loudonville, NY 12211 Email: rfinn@siena.edu
[2] NSF Astronomy and Astrophysics Postdoctoral Fellow
[3] Department of Physics, University of Waterloo, Waterloo, Canada N2L 3GI Email: mbalogh@uwaterloo.ca
[4] Steward Observatory, 933 N. Cherry Ave., University of Arizona, Tucson, AZ 85721 Email: dzaritsky@as.arizona.edu
[5] NOAO Cerro Tololo Inter-American Observatory, 950 North Cherry Avenue, Tucson, AZ 85719, Email: cmiller@noao.edu
[6] Institute of Cosmology and Gravitation, University of Portsmouth, Portsmouth, UK, P01 2EG Email: bob.nichol@port.ac.uk

cused on trying to disentangle the effects of galaxy stellar mass from those of environment (e.g. Kauffmann et al. 2004; Weinmann et al. 2006a; Baldry et al. 2006). In the present paper our goal is to understand how the total Hα luminosity in clusters, integrated over all bright galaxies, depends on cluster velocity dispersion. This allows us to make a direct comparison with higher-redshift studies, and therefore begin to construct a star-formation history for galaxies in clusters analogous to what has been done in the field (e.g. Madau et al. 1998; Hopkins 2004). Some attempt at this has already been made (Poggianti et al. 2006; Nakata et al. 2005); here we expand on these works, using a larger sample of local clusters with reliable velocity dispersions and Hα emission-line measurements.

Specifically, we investigate star-formation as traced by Hα in 308 low-redshift clusters drawn from the C4 cluster catalog (Miller et al. 2005). We describe the cluster sample selection in §2 and the selection of Hα-emitting galaxies in §3. We quantify the mass-dependence of cluster star-formation rates in §4, and use these results to quantify the environment-dependent evolution by comparing with a higher-redshift sample of clusters in §5. We summarize the main results and present conclusions in §6. We adopt a ΛCDM cosmology, assuming $\Omega_0 = 0.3$, $\Omega_\Lambda = 0.7$, and $H_0 = 70$ km s^{-1} Mpc^{-1} unless otherwise noted.

2. CLUSTER SAMPLE & MEMBER GALAXIES

2.1. *Sample Selection*

We select our cluster sample from the C4 DR5 cluster catalog (Miller et al. 2005). We apply a minimum redshift cut of $z = 0.05$ to minimize aperture effects of the fiber spectra (Kewley et al. 2005) and a maximum redshift cut of 0.09 to minimize incompleteness of the galaxy catalog due to the spectroscopic magnitude limit. This leaves a sample of 923 clusters.

The virialized region of a cluster scales with cluster mass, so we need a reliable mass estimate in order to properly select member galaxies for each cluster. There are many ways to estimate cluster mass. For example, Weinmann et al. (2006b) estimate halo mass using halo occupation models, and Rines & Diaferio (2006) use the distribution of galaxies in $\Delta v - \Delta r$ space to derive cluster mass profiles. However, the simplest method, and the one most easily applied to higher redshift samples, is to use the cluster velocity dispersion. Velocity dispersion can be an accurate tracer of cluster mass for relaxed systems that are not dominated by substructure, and for which there are a sufficiently large number of redshifts available (e.g., Miller et al. 2005). Furthermore, velocity dispersion can be directly related to other cluster properties such as virial radius using the virial theorem and cluster size in the redshift dimension assuming an underlying velocity distribution.

We will therefore use velocity dispersion as a measure of cluster mass. However, for this approach to be valid a minimum requirement is that the clusters be in approximate virial equilibrium, with a well-defined measurement of velocity dispersion. To satisfy this condition, we exclude clusters which do not appear to be dynamically relaxed. This selection may reduce the scatter in cluster properties at fixed mass compared with an unbiased sample. It may also bias the average star-formation rates, if cluster mergers directly affect star formation in member galaxies. However the advantage is that we can more directly identify any correlations with system mass, independently of dynamical effects. Clusters with no significant substructure should have velocity distributions that are nearly gaussian, and we identify unrelaxed clusters by quantifying how much their velocity distribution deviates from this. For each cluster, we fit a gaussian with a width equal to the cluster velocity dispersion from Miller et al. (2005). We normalize the gaussian so that the area within $\Delta v < 2\sigma$ matches the observed number of cluster members in that velocity range. To illustrate, we show the velocity distributions and gaussian fits for the first twenty clusters in Figure 1.

We use the χ^2_ν statistic to quantify the deviation of the velocity distribution from gaussian, where

$$\chi^2_\nu = \frac{1}{(N_{bin} - 3)} \sum_{i=1}^{N_{bin}} \frac{(N_{obs} - N_{gauss})^2}{\sigma^2_{N_{obs}}}. \qquad (1)$$

N_{bin} is the number of bins, N_{obs} is the number of galaxies observed in each bin, N_{gauss} is the number of galaxies expected in a gaussian distribution, and $\sigma_{N_{obs}} = \sqrt{N_{obs}}$ is the error associated with the expected counts. When N_{obs} is zero, we set $\sigma_{N_{obs}}$ to 1. We use a bin size of 0.3 times the velocity dispersion. After visual inspection of the velocity histograms, we find that $\chi^2_\nu < 2.0$ excludes clusters with significant substructure within the cluster itself or in the nearby environment. If a cluster does not make the χ^2_ν cut, we try recentering the velocity distribution and then recalculate χ^2_ν. If χ^2_ν of the recentered distribution meets the criteria, we keep the cluster and the new central velocity.

The χ^2_ν criteria is not uniform with velocity dispersion; χ^2_ν is systematically lower for clusters with lower numbers of galaxies. Therefore, we impose a minimum velocity dispersion of 450 km s^{-1} because the χ^2_ν cut becomes unreliable below this point, leaving a sample of 452 clusters. In addition, we note that at all values of velocity dispersion this cut will preferentially select clusters with fewer galaxies, and we must keep this selection effect in mind when interpreting our results.

We apply the $\chi^2_\nu < 2.0$ criteria to the remaining clusters with $\sigma > 450$ km s^{-1}, which leaves 308 clusters. We show velocity dispersion versus redshift for the final sample of clusters in Figure 2. There is no trend in velocity dispersion versus redshift for the final sample.

2.2. *Cluster Membership*

The size of the virialized region of a cluster scales with cluster mass. Therefore, our radial cut for selecting cluster members must scale with cluster mass to sample analogous regions of each cluster. We characterize the radial extent of each cluster in terms of R$_{200}$, which is the radius inside which the enclosed density is 200 times the critical density and approximates the virial radius of the cluster. Using the redshift dependence of the critical density and the virial mass to relate line-of-sight velocity dispersion, σ_x, to cluster mass, we express R$_{200}$ as:

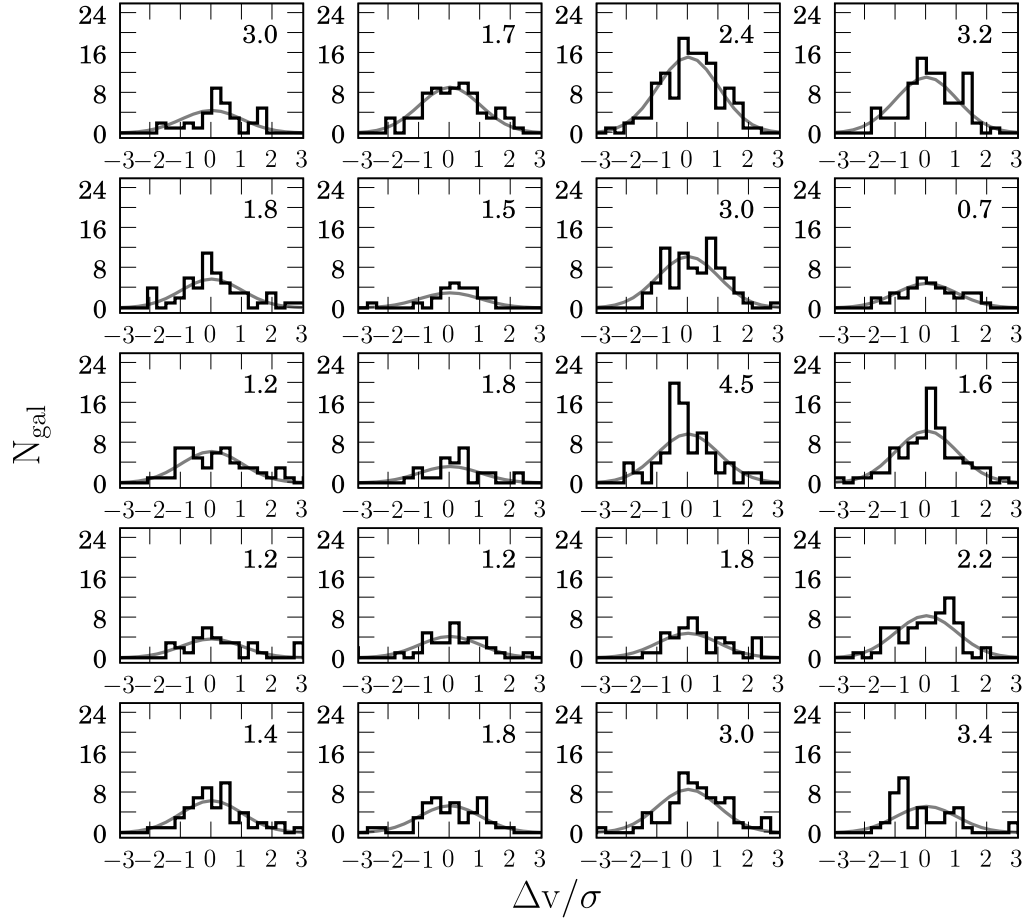$$R_{200} = \sqrt{\frac{9}{800 \pi G \rho_c(z)}} \, \sigma_x, \qquad (2)$$

FIG. 1.— Velocity histograms for first 20 clusters. The gray curve shows a gaussian with width equal to the cluster velocity dispersion and normalized so that the area within 2σ matches the observed number of galaxies in the same velocity slice. The number in the upper right of each panel is the value of χ^2_ν. Clusters with $\chi^2_\nu > 2.0$ are rejected due to the presence of significant substructure within or near the cluster.
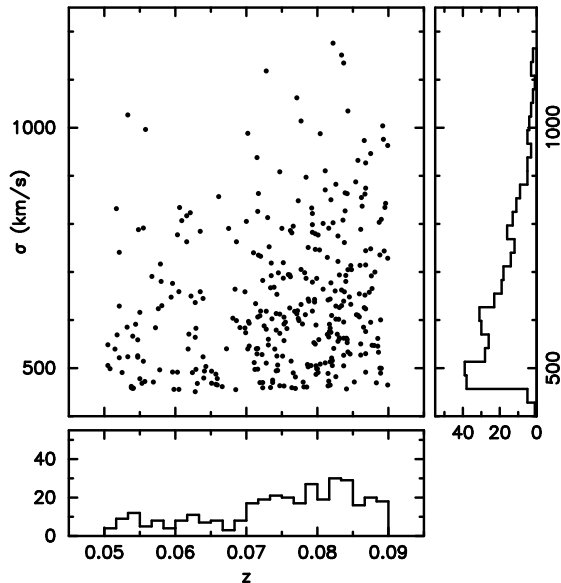
FIG. 2.— Cluster velocity dispersion versus redshift. The bottom panel shows a histogram of number of clusters versus redshift. The side panel shows the histogram of number of clusters versus velocity dispersion.

where the critical density, $\rho_c(z)$, is given by the following equation:

$$\rho_c(z) = \frac{3\,H_0^2}{8\,\pi\,G}\,(\Omega_\Lambda + \Omega_0(1+z)^3). \qquad (3)$$

Simplifying, we can write R_{200} as

$$R_{200} = 2.02\,\frac{\sigma_x}{1000\text{ km/s}}\,\frac{1}{\sqrt{\Omega_\Lambda + \Omega_0(1+z)^3}}\,h_{70}^{-1}\text{ Mpc}. \qquad (4)$$

In deriving Equation 2 we have implicitly assumed that galaxies are orbiting isotropically in a single isothermal sphere potential, so σ_x is related to the circular velocity V_c by $\sigma_x = V_c/\sqrt{2}$.

We use the mock galaxy redshift survey of Yang et al. (2004) to help define the optimal selection of cluster members in velocity space. We use the 300 h^{-1} Mpc simulation and select all halos with masses greater than 10^{14} M$_\odot$ so that the minimum mass of the mock clusters is consistent with the mass threshold imposed on the SDSS clusters by our $\sigma > 450$ km s^{-1} cut. This results in 1062 virialized clusters containing a total of a half million galaxies. The velocity distributions of the mock clusters are defined to be gaussian. Thus the mock clusters should be comparable to our cluster sample because we exclude clusters whose velocity distributions deviate significantly from gaussian. We then select galaxies around each halo that have $M_{B_J} < -18$ and velocities within $\pm 3\sigma$ of the central velocity. In the top panels of Figure 3, we show the fraction of observed galaxies that are members (solid line) and non-members (dotted line) in each radial bin as a function of projected distance from the cluster center, where members are those galaxies physically located within the virial radius of the cluster. Yang et al. define the virial radius using R_{180}; their definition of R_{vir} is thus 5% larger than our value of R_{200}, but this slightly larger radial cut does not significantly affect the results. The left panel of Figure 3 shows completeness

and contamination for all galaxy types, and the number of contaminating galaxies exceeds the number of member galaxies at a radius of 0.9 times the virial radius. The right panel shows completeness and contamination for late-type galaxies only, with the number of contaminating late-type galaxies exceeding the number of member late-type galaxies at a projected radius of 0.7 times the virial radius. In the bottom panel of Figure 3, we show the fraction of members and non-members per bin as a function of velocity cut, including all galaxies with a projected separation less than R_{vir}. For a gaussian distribution of velocities, a 2σ membership cut within the virial radius provides fairly high completeness ($\geq 95\%$), while increasing the velocity cut to 3σ adds more non-members than members. When working within R_{200}, we therefore limit our analysis to galaxies within 2σ. Note that the results are not sensitive to the magnitude cut; we find no significant difference for magnitude cuts ranging from $M_{B_J} < -16$ to $M_{B_J} < -19$. Thus, while a magnitude cut of $M_{B_J} = -19$ is more comparable to the r-band magnitude cut we impose (as discussed below), the $M_{B_J} = -18$ allows us to increase signal-to-noise without affecting the results.
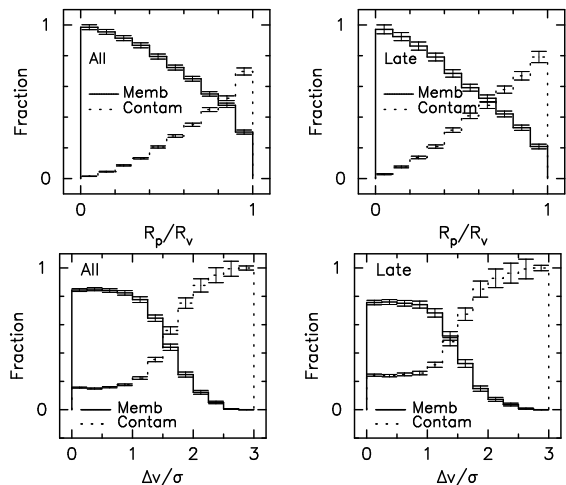

FIG. 3.— The fraction of members (solid curve) and non-members (dashed line) per bin as a function of projected cluster-centric radius, R_p, normalized by the virial radius (top panels) and velocity cut, Δv, normalized by the cluster velocity dispersion (bottom panels) in the Yang et al. (2004) model. The left panels show all galaxies and the right panels show late-type galaxies only. The errorbars show the $1-\sigma$ Poisson noise associated with the galaxy number counts.

Finally, we apply an absolute magnitude cut of $M_R \leq -20.68$ to the cluster galaxies. This corresponds to the spectroscopic completeness limit of $r = 17.77$ at $z = 0.09$, the maximum redshift of our cluster sample. The absolute magnitude cut takes into account the maximum k-correction possible (Blanton et al. 2003a). Note that this is only about 0.5 magnitudes fainter than the characteristic luminosity M^* (Blanton et al. 2003a). Our analysis is therefore restricted to relatively bright galaxies, and it should be kept in mind that star formation activity can be substantially higher for less massive galaxies (e.g. Baldry et al. 2006).

2.3. *Control Sample*

We construct a control (field) sample to compare with our cluster measurements and to check for systematic effects in our analysis. For each cluster, including those with substructure, we center on a random galaxy within the DR5 redshift survey area, *regardless of its magnitude*, and we avoid centering near clusters. We then select surrounding galaxies with magnitudes brighter than $M_R = -20.68$ that lie within R_{200} and $\Delta v \leq 2\sigma$. We select five such randomly positioned samples for each cluster, resulting in a control sample of 2260 independent pointings. We generate control samples for clusters that meet the redshift cuts and lower velocity dispersion limit cut. However, we do not limit the control sample based on the substructure of its parent cluster. As a result, the control sample spans a slightly different range of velocity dispersion than the cluster sample.

2.4. *Correction for Incomplete Fiber Sampling*

Not all cluster members are targeted by SDSS spectroscopy, so we must correct the cluster and control samples for incomplete spectroscopic sampling when calculating integrated cluster properties such as the number of galaxies, total stellar mass, and total star-formation rate. To estimate the completeness of the spectroscopic sampling, we count the number of galaxies in the photometric catalog with an r-band magnitude greater than that corresponding to $M_r = -20.68$ at the cluster redshift. We compare this to the number of galaxies with spectra in the same region and magnitude slice, and multiply the integrated cluster properties by the ratio of photometric to spectroscopic sources. For the cluster sample, the average completeness is 0.86 ± 0.15, 0.86 ± 0.11, and 0.87 ± 0.10 for radial cuts at 0.5, 1.0, and $2.0 \times R_{200}$. The median completeness is 0.89. For the control sample, the average completeness within 0.5, 1, and $2 \times R_{200}$ is $0.92 \pm 0.20, 0.89 \pm 0.16$, and 0.88 ± 0.12. The completeness estimates for the control fields are in good agreement with the expected spectroscopic completeness of 90% (Blanton et al. 2003b), while the completeness estimates for the clusters are slightly lower due to the higher density of sources.

3. STAR-FORMING GALAXIES

3.1. *Definition of Star-Forming Galaxies*

We require star-forming galaxies to have Hα luminosities greater than 0.41×10^{40} ergs s^{-1} to sample the same fraction of the Hα luminosity function in each cluster. This limit corresponds to the minimum Hα flux detected at $z = 0.09$, $f_{H_\alpha} = 2.0 \times 10^{-16}$ ergs s^{-1} cm^{-2}, which we determine empirically. This luminosity limit corresponds to a SFR of 0.08 h_{100}^{-2} M$_\odot$ yr^{-1} if we assume a typical extinction value of 1 magnitude at Hα (Kennicutt et al. 1994).

We also require star-forming galaxies to have a rest-frame Hα equivalent width greater than 4Å, which allows us to minimize contamination from uncertainties on the line width measurements and stellar absorption of inactive galaxies (e.g. Balogh et al. 2004). However, imposing this cut necessarily means we will underestimate the total amount of star formation in an Hα flux-limited sample. To test this, we consider the subsample of galaxies with $z < 0.075$, where we can reliably push to lower EW limits. We find that at most 5% of the total star formation in our flux-limited sample occurs at

EW< 4Å. As this small contribution is somewhat uncertain (since measurement uncertainties and stellar absorption still play a role) we do not correct for it.

We exclude AGN from the sample of star-forming galaxies using the AGN classification provided by Miller et al. (2003), which have been updated to include the DR5 galaxies. We find $22 \pm 13\%$ of galaxies by number with significant AGN emission within $\Delta v < \pm 2\sigma$ and $1 \times R_{200}$, and they contribute an average(median) of $21 \pm 13\%(29\%)$ of the total Hα flux. This result is consistent with the AGN fraction measured by Miller et al. (2003) and Kauffmann et al. (2003a).

3.2. *Star-Formation Rates & Stellar Mass*

To calculate SFR from observed Hα flux, we first apply an aperture correction which is computed by comparing the flux within the R-band petrosian radius with the flux in the fiber radius (Balogh et al. 2004). We then convert Hα flux to luminosity by multiplying by $4\pi d_L^2$, where d_L is the luminosity distance. We use the Kennicutt star-formation relation (Kennicutt et al. 1994) to convert Hα luminosity to SFR, where

$$1 \text{ erg s}^{-1} = 7.9 \times 10^{-42} \text{ M}_\odot \text{ yr}^{-1}. \qquad (5)$$

We correct for extinction using values of A$_z$ from Kauffmann et al. (2003b), assuming the extinction law is of the form $\tau_\lambda \propto \lambda^{-0.7}$ and thus $A_r = A_z + 0.23$. The Kauffmann et al. sample has been updated to include DR4 galaxies but not DR5. Therefore, 23% of the galaxies do not have an extinction value from these catalogs. To estimate the extinction for these galaxies, we use the DR4 galaxies to define a relationship between A$_r$ and M$_r$. The median value of A$_r$ for galaxies brighter than our magnitude cut (M$_r < -20.68$) remains fairly constant at a value of 0.76 magnitudes. Therefore, we assume 0.76 magnitudes of extinction at Hα for the galaxies not included in the Kauffmann et al. (2003b) catalog. The standard deviation in A$_r$ about the mean is 0.30 magnitudes, and changing the extinction value by one standard deviation alters the inferred star-formation rates by 30%. Thus, the error associated with the extinction correction is small compared to other sources of error and does not significantly affect our results.

Stellar mass is the integral of a galaxy's star-formation history and enables us to study past star-formation efficiency as a function of cluster mass. Again, we use stellar mass estimates from Kauffmann et al. (2003b). To estimate the stellar mass for galaxies not included in the Kauffmann et al. catalog, we use the DR4 galaxies to define a relation between M$_r$ and stellar mass. We show the result in Figure 4, where the blue line shows the relationship we use for galaxies with M$_r > -21.5$ (blue line) and the cyan line shows the slightly flatter relationship for galaxies with M$_r < -21.5$.

4. MASS DEPENDENCE OF CLUSTER SF PROPERTIES

We first investigate how the number of cluster members brighter than $M_r = -20.68$ depends on cluster velocity dispersion. In Figure 5, we show the number of galaxies within R$_{200}$ and with $\Delta v < 2\sigma$ for the cluster (black circles) and control fields (open squares). The small black points show the values for the individual clusters. The number of galaxies is strongly correlated with
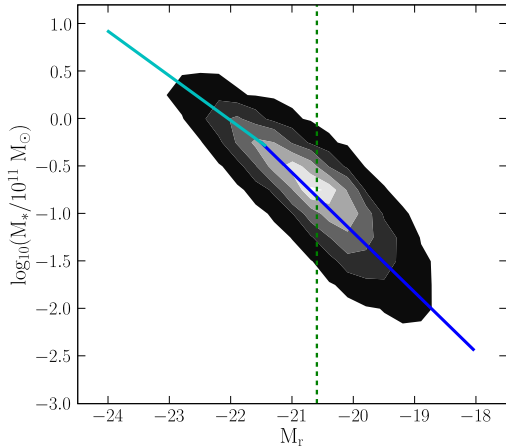
FIG. 4.— Distribution of stellar mass versus M_r for the DR4 galaxies. Blue and cyan line show average relation used to estimate stellar mass from M_r for galaxies not included in the Kauffmann et al. (2003b) catalogs. The dashed green vertical line shows the magnitude cut used when selecting cluster members.

velocity dispersion for both samples. Note that the number of galaxies in the control sample increases as approximately σ^3 as expected since the cylindrical selection volume scales in this way. The cluster fields are overdense relative to the field, by a factor of 6—23 that appears to depend on velocity dispersion. Note that the clusters are not corrected for residual field contamination; this figure demonstrates that we are overestimating the number of cluster galaxies by no more than about 10 per cent due to this effect. The filled squares show the control data rescaled by a factor of 7.8, to allow easy comparison of the slope of the cluster and control samples.
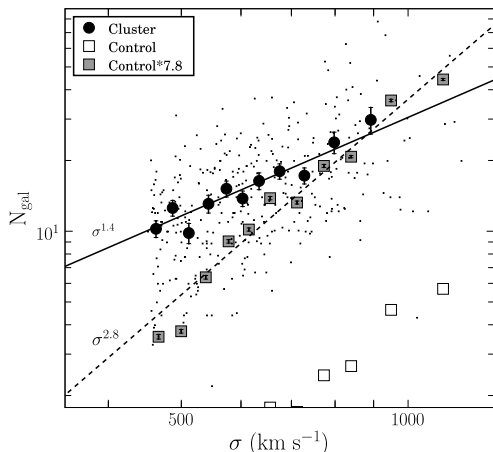

FIG. 5.— The total number of galaxies as a function of cluster velocity dispersion for all galaxies with velocities within $\pm 2\sigma$ and projected cluster-centric distance less than $1 \times R_{200}$. The small black points show the values for individual clusters, and the larger symbols show the average in equally populated bins for the cluster (black circles) and control (open squares) samples. Errorbars show the error in the mean in each bin. The filled squares show the control data, scaled so that the average counts in the control fields equal the average counts in the cluster fields. The solid line shows the best power-law fit for the cluster data, and the dashed line shows the best power-law fit for the control data.

It is evident that the number of galaxies in the cluster fields follows a flatter trend versus velocity dispersion than the number of galaxies in the control fields. However, we note that there are several important biases here that must be accounted for. First, the uncertainties on both values are correlated, such that an overestimated σ leads to a larger volume and, hence, an overestimated $N_{\rm gal}$. For the field sample, the uniform galaxy density means one expects $N_{\rm gal} \propto \sigma^3$, so $dN_{\rm gal} \propto \sigma^2 \, d\sigma$. However, for the cluster population, the galaxy overdensity in a given cluster is expected to decline as approximately R^{-2}, so the total number of galaxies within R_{200} (which includes the cluster and surrounding field population) should scale like $N_{\rm gal} \propto \sigma^\alpha$, with $\alpha < 3$. At the extreme, where the background population is negligible and most of the cluster population is well within R_{200}, $N_{\rm gal}$ is independent of uncertainties in σ. For these reasons, at a fixed value of σ, observational uncertainties alone will scatter the cluster measurments of $N_{\rm gal}$ along a slope that is shallower than that of the field measurements. We do not attempt to quantify this however, as it is sensitive to the radial distribution of galaxies within clusters, and the relative contribution of foreground and background galaxies. Finally, cluster selection biases will play a role. The imposed limit on σ results in a bias at low σ toward clusters where σ is overestimated. Furthermore, our χ^2 cut on velocity distribution tends to favor systems with fewer members, which will result in a bias at high σ toward fewer $N_{\rm gal}$. For all these reasons we do not attribute much significance to the apparently flatter slope of the clusters. Hereafter, when attempting to quantify cluster star-formation properties as a function of σ, we will normalize by the total number of member galaxies so that we reduce the σ-dependence of the dependent variable. Similar results would be obtained if we normalized by the total stellar mass (we will show below that the two are strongly correlated, as expected); however for comparison with high-redshift studies it is preferable to use a simple measurement like $N_{\rm gal}$ if possible.

4.1. Distribution of Hα Luminosities

We show the distribution of Hα luminosities as a function of cluster velocity dispersion in Figure 6. We split the cluster sample into three groups based on mass, and dividing at $\sigma = 575$ km s^{-1} and $\sigma = 700$ km s^{-1} yields an approximately equal number of galaxies per group (~ 800). The points (stars, open circles, open triangles) show the number of galaxies per luminosity bin divided by the total number of galaxies in that mass division (~ 800 galaxies), and the errorbars show the $1 - \sigma$ Poisson noise. The three sets of points are consistent within the errors, showing that the distribution of Hα luminosities is not a strong function of cluster velocity dispersion.

In Figure 7, we compare the distribution of Hα luminosities for the cluster (stars) and control (filled circles) samples. The open circles show the distribution for the control fields after being scaled to meet the average counts of the cluster fields. The errorbars for the cluster and scaled control fields overlap, indicating that the shapes of the cluster and control Hα luminosity distributions are similar. This implies that the primary difference between the cluster and control sample is in the fraction of star-forming galaxies, with the star-forming fraction of
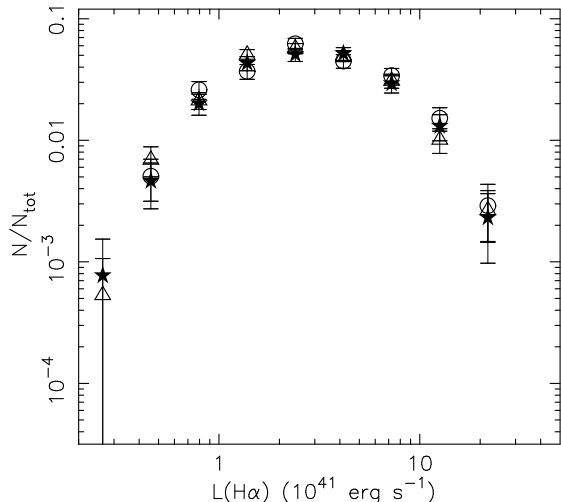
FIG. 6.— Number of galaxies per bin divided by total number of galaxies versus L(Hα). Stars, circles, and triangles show galaxies from clusters with $\sigma < 575$, $575 \leq \sigma < 700$, and $\sigma \geq 700$ km s^{-1}, respectively. Errorbars reflect $1 - \sigma$ Poisson noise.

the control fields a factor of ~ 1.6 higher than the cluster fields. This is consistent with previous results based on smaller samples (Carter et al. 2001; Balogh et al. 2004; Rines et al. 2005), which have shown that the distribution of Hα luminosities and EWs of the star-forming population is independent of environment.
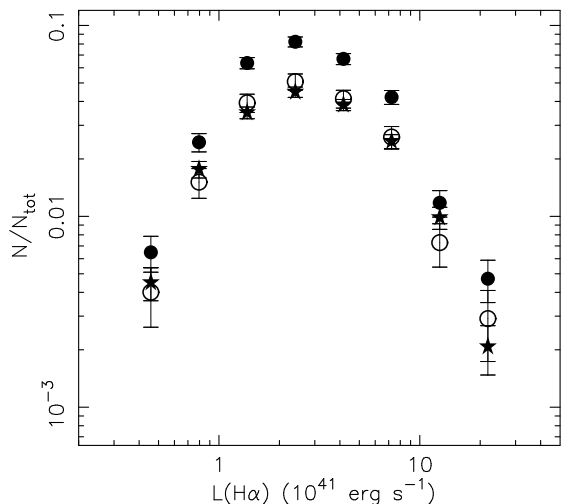

FIG. 7.— Number of galaxies per bin divided by total number of galaxies versus L(Hα) for the cluster (star) and control (filled circles) samples. The open circles show the distribution for the control fields after being scaled to meet the average counts of the cluster fields. Errorbars reflect poisson noise. The

4.2. *Integrated Cluster Properties*

We now look for a mass dependence in the integrated properties of the star-forming cluster galaxy population. In Figure 8, we show the total stellar mass (panel 1), the number of star-forming galaxies (panel 2), and the total SFR (panel 3) for all galaxies within R_{200} and with $\Delta v < 2\sigma$ versus cluster velocity dispersion, where all the dependent variables have been normalized by the number of galaxies in each cluster to reduce our sensitivity to

correlated errors. The left and right columns of Figure 8 show the cluster and control data, respectively. The small black points show the values for individual fields, and the filled circles show the average in equally populated bins. The errorbars, often smaller than the filled circles, show the error in the mean. The solid line shows the best power-law fit in each panel, and the dashed horizontal line shows the average value to show what one would expect if there is no dependence on cluster mass. None of the power-law fits deviates significantly from a flat relationship, indicating all three measures of star-formation efficiency are independent of cluster mass, at least for clusters with $\sigma > 450$ km s^{-1}. An equivalent way to express these results is that the total stellar mass, the number of star-forming galaxies, and the total SFR scale linearly with the number of galaxies, independent of cluster velocity dispersion.

Our results are generally consistent with those of other studies that have measured star-formation efficiency as a function of cluster mass using smaller samples of SDSS clusters. Poggianti et al. (2006) use a smaller subset of the C4 clusters and find that the fraction of star-forming galaxies decreases as velocity dispersion increases from $\sim$300 to $\sim$500 km s^{-1} and then levels off. We do not probe to low enough velocity dispersions to compare results at $\sigma = 300$ km s^{-1}, but our results are consistent with a flat relationship for $\sigma > 450$ km s^{-1}. Note that this result is unchanged if we keep AGN in our sample (e.g. Poggianti et al. 2006). These results are fully consistent with the lack of mass dependence observed from smaller samples of both optically-selected (Goto 2005) and X-ray selected (Popesso et al. 2007) clusters.

5. EVOLUTION OF CLUSTER STAR FORMATION

We now use our SDSS cluster sample as a low-redshift baseline and compare with star-formation properties of higher-redshift clusters from the literature. We will focus on those few studies that have comparably complete observations of Hα emission.

There are a growing number of Hα surveys of galaxy clusters at $z > 0.1$, including both spectroscopic (Couch et al. 2001; Balogh et al. 2002) and narrow-band imaging (Balogh & Morris 2000; Finn et al. 2004; Kodama et al. 2004; Finn et al. 2005) surveys, which are suitable for our purposes. For this comparison we use only the narrow-band Hα imaging data for three $z \simeq 0.75$ clusters from Finn et al. (2005) because they provide the longest redshift baseline and the narrow-band observations for all three clusters were made in a uniform way using the same telescope and near-infrared camera. In addition, the three clusters are from the ESO Distant Cluster Survey (EDisCS; White et al. 2005), and so they have readily available derived-data products (such as k-corrected absolute magnitudes and estimates of the total number of member galaxies; Pelló et al. 2007; Rudnick et al. 2007) that enable a more precise comparison with the SDSS clusters. Furthermore, spectroscopic (Halliday et al. 2004; Milvang-Jensen et al. 2008), weak lensing (Clowe et al. 2006), and X-ray studies (Johnson et al. 2006) show that the velocity dispersions provide a reliable estimate of cluster mass for these clusters. The EDisCS clusters CL 1040−1155, CL 1054−1245, and CL 1216−1201 are at redshifts of 0.704, 0.748 and 0.794, respectively. Note that we do not have the data nec-
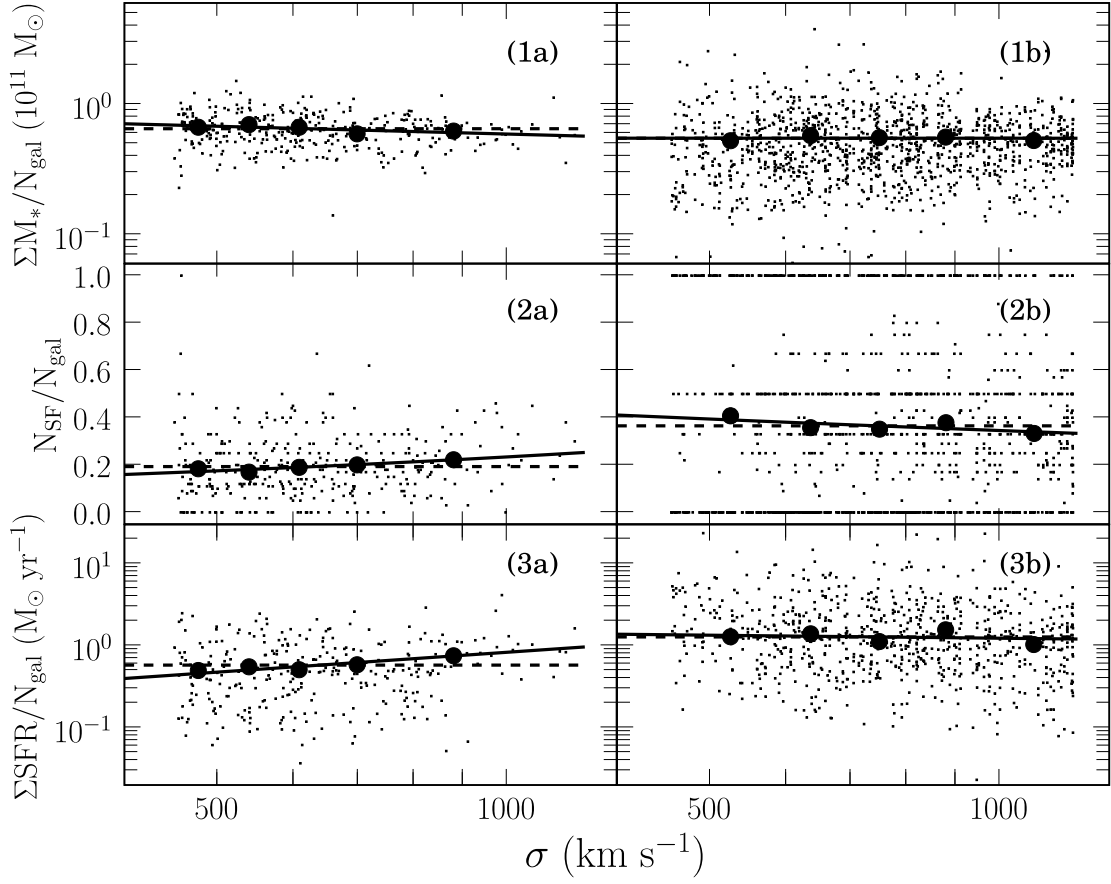
FIG. 8.— (1) Total stellar mass, (2) number of star-forming galaxies, and (3) the total SFR per total number of galaxies versus cluster velocity dispersion for all galaxies with velocities within $\pm 2\sigma$ and projected cluster-centric distance less than $1 \times R_{200}$. The left and right panels show the cluster and control data, respectively. In each panel, the small black points show the values for individual clusters or control fields, and the larger symbols show the average in equally populated bins. Errorbars showing the error in the mean in each bin are smaller than the symbols. The solid line shows the best power-law fit for the data, and the dashed line shows the average value of the y-axis variable.

essary to identify AGN in the $z \simeq 0.75$ clusters. As a result, we include SDSS galaxies with AGN emission as well, and hereafter we discuss Hα emission in terms of L(Hα) rather than SFR.

5.1. Integrated Hα Luminosity

The integral of the Hα luminosity function gives the total Hα luminosity per cluster or integrated SFR if AGN are excluded. This quantity is analogous to the volume-averaged SFR that is commonly used to quantify the evolution of field galaxies (e.g., Madau et al. 1998; Hippelein et al. 2003; Hopkins 2004), and so we use the total Hα luminosity as a means of quantifying the evolution between the SDSS and $z \simeq 0.75$ clusters.

When calculating the integrated Hα luminosity, we apply several selection criteria to ensure that we are comparing complete and analogous galaxy samples in the higher and low-redshift clusters. First, we apply the same radial and velocity cuts to all clusters, including all galaxies within $0.5 \times R_{200}$ and $\Delta v < 3\sigma$. The radial cut matches the areal coverage of the EDisCS clusters, and the velocity cut matches the filter width for CL 1216$-$1201. The filters for CL 1040$-$1155 and CL 1054$-$1245 correspond to a velocity width closer to 6σ. The correction for the extra field contamination in these filters, which we detail in the Appendix, amounts to scaling the integrated L(Hα) of CL 1040$-$1155 and CL 1054$-$1245 by a factor of 0.81. Second, we apply the same rest-frame equivalent width cut of 10Å to all star-forming galaxies, which is the minimum Hα equivalent width detected in the $z \simeq 0.75$ narrow-band imaging surveys. Third, we include only those galaxies with $M_r < -20.68$, where the values of M_r for the EDisCS clusters are taken from Pelló et al. (2007). Fourth, we require the SDSS galaxies to have Hα luminosities that lie above the flux limit of the $z \simeq 0.75$ Hα imaging, which we discuss in more detail in §5.2. Finally, we correct the integrated L(Hα) of the SDSS clusters by the spectroscopic completeness as described in §2.4.

The cluster version of the Madau plot (Madau et al. 1998) needs to take into account that the integrated Hα luminosity scales with cluster mass. Therefore, instead of showing integrated Hα luminosity versus redshift, we show ΣL(Hα) versus cluster velocity dispersion in Figure 9 and measure an offset between the low and high-redshift cluster samples. The open circles show the average ΣL(Hα) in equally-populated bins versus velocity dispersion for the SDSS clusters, and the errorbars show the error in the mean. The filled points show ΣL(Hα) for each individual high-redshift cluster, and the errorbars are the uncertainty of the sum. The bold solid lines in Figure 9 show a slope of 2.9, which is the best-fit slope derived from the SDSS clusters. We assume the same slope for the $z \simeq 0.75$ clusters and fit the zeropoint by least-squares minimization. The thin dotted lines show the standard deviation associated with zeropoint for both the SDSS and EDisCS power-law as determined by bootstrap resampling. The offset between the best-fit lines for the SDSS and $z \simeq 0.75$ clusters corresponds to a factor of $\sim$26$\pm$16 increase in ΣL(Hα) when measured at a fixed velocity dispersion, with the uncertainty dominated by the uncertainty in the high-redshift zeropoint. Clusters evolve, however, and a typical cluster has roughly doubled its mass since $z \simeq 0.75$. The gray solid lines in Fig-

ure 9 link the $z = 0.07$ clusters with their progenitors at $z = 0.75$, where we have used the semi-analytic models of Wechsler et al. (2002) to estimate the redshift-evolution of cluster mass. Taking the mass evolution into account, the inferred evolution for a given cluster is a median factor of $\sim 10 \pm 6$, with the amount of evolution increasing as cluster mass decreases.
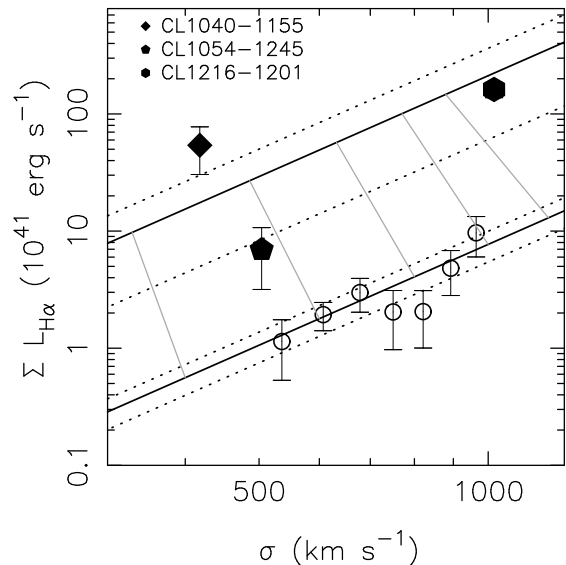

FIG. 9.— Integrated Hα luminosity versus cluster velocity dispersion for C4 clusters (open circles) and $z \simeq 0.75$ EDisCS clusters (filled symbols). The solid black lines show a slope of 2.9, which is the best-fit slope derived from the SDSS clusters. The dotted lines show the standard deviation associated with the zeropoint of powerlaw fits. The solid gray lines link the $z = 0.07$ clusters with their progenitors at $z = 0.75$.

To measure the average evolution in the total Hα luminosity between the SDSS and higher-redshift clusters, we assume that the slope of the $\Sigma L(H\alpha) - \sigma$ relation is the same for the SDSS and higher-redshift clusters. The change in zero point then indicates the average evolution. However, the slope of the relation could also vary with redshift. For example, Poggianti et al. (2006) present a detailed analysis of the star-forming population for the complete EDisCS sample of 17 $0.4 < z < 0.8$ clusters, and their results suggest that the trend of total star-formation rate versus cluster mass is flatter at higher redshift. Poggianti et al. use the [O II] emission line as a star-formation indicator, and here we limit our comparison to the 3 EDisCS clusters that have Hα luminosities. As a result of the small sample size, we can not independently measure the dependence of star formation on cluster mass for the high-redshift sample. However, because the SDSS and 3 EDisCS clusters presented here span the same range of velocity dispersions, the zeropoint calculation will yield a similar number even if the slope of the relation changes with redshift. Thus our measure of the average evolution in the total Hα luminosity between $z = 0.07$ and $z \simeq 0.75$ should be insensitive to changes in the slope of the $\Sigma L(H\alpha) - \sigma$ relation, although the interpretation of this result could be different.

As with the analysis in §4.2, we try to reduce the dependence of the dependent variable, the integrated Hα luminosity, on σ by normalizing by the total number of member galaxies. For the EDisCS clusters, we use the

estimate of the total number of galaxies that is derived from the luminosity functions of Rudnick et al. (2007); these estimates have associated uncertainties of 30-50%. The results, shown in Figure 10, indicate that the average Hα luminosity per galaxy has increased by a factor of 13 ± 7 between $z \simeq 0.07$ and $z \simeq 0.75$. We show the fraction of star-forming galaxies versus redshift in Figure 11. The fraction of star-forming galaxies (where star-forming galaxies are those that meet the selection criteria outlined above) is a factor of 6 ± 3 higher in the EDisCS clusters. Poggianti et al. (2006) find that the fraction of star-forming galaxies varies with cluster mass at higher redshift. Again, we are comparing with only 3 higher-redshift clusters, and so we do not attempt to quantify a mass-dependent evolution in the star-forming fraction.
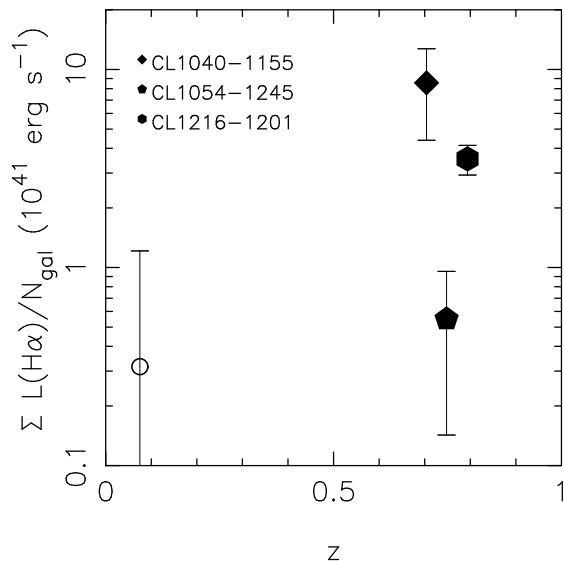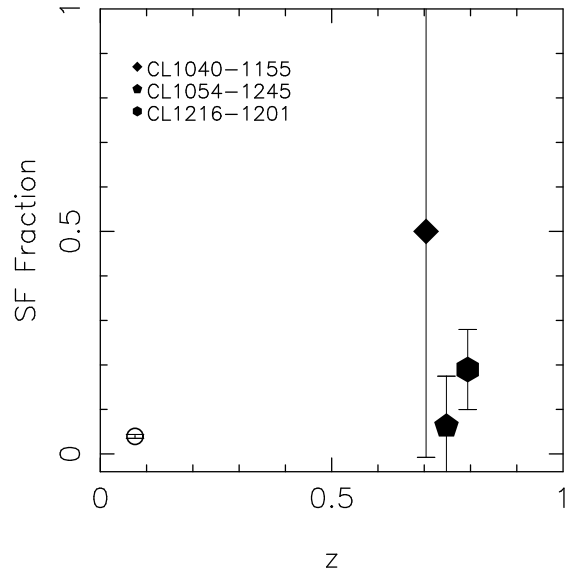

FIG. 11.— Fraction of star-forming galaxies versus cluster redshift for C4 clusters (open circle) and $z \simeq 0.75$ EDisCS clusters (filled symbols).

FIG. 10.— Integrated Hα luminosity divided by number of member galaxies versus cluster redshift for C4 clusters (open circle) and $z \simeq 0.75$ EDisCS clusters (filled symbols). The point for the C4 clusters shows the average for the 308 clusters, and the errobars show the standard deviation.

5.2. *Distribution of Hα Luminosities*

We now try to understand the global evolution of cluster star-formation properties in terms of the evolution of individual star-forming galaxies. We show the low and high-redshift star-forming galaxies in Figure 12, where we plot L(Hα) versus M$_r$ in panel (1a) for all galaxies within $0.5 \times$R$_{200}$ and $\Delta v < 3\sigma$. The black points show the galaxies in the 308 SDSS clusters and the filled stars show the galaxies in the three $z \simeq 0.75$ clusters (we do not correct for the additional field contamination in CL 1040−1155 and CL 1054−1245). The dotted line in Figure 12 shows the approximate flux limit of the $z \simeq 0.75$ imaging, and the dashed vertical line shows the magnitude corresponding to the SDSS spectroscopic completeness limit. The solid gray line shows the approximate effect of imposing a minimum Hα EW cut of 4Å for the SDSS galaxies. The galaxies that meet the high-redshift flux limit and the SDSS spectroscopic magnitude cut are shown in panel (1b) of Figure 12.

To compare the distribution of Hα luminosities, we consider only the star-forming galaxies that lie above the

high-redshift flux limit and are brighter than the SDSS spectroscopic limit (shown in panel (1b), Figure 12) so that we are comparing relatively complete populations in both cluster samples. In panel (1c) we show the number of galaxies per bin divided by the total number of cluster members versus L(Hα) for the SDSS galaxies (open circles) and EDisCS galaxies (filled stars). The high-redshift clusters contain a higher fraction of the star-forming galaxies. This could be explained by pure number evolution, if the fraction of star-forming galaxies per cluster increased by a factor of ~ 10, with no change in the distribution of Hα luminosities of star-forming galaxies. However, the SDSS L(Hα) distribution peaks at a lower value of L(Hα) than the EDisCS distribution, indicating that there is some evolution of the Hα luminosities of individual galaxies.

As an example of evolution that is due solely to an increase in the average star-formation rate per galaxy (among the active population), we simply scale the Hα luminosities of individual SDSS galaxies by a factor of 10, which is the amount of evolution observed in the integrated Hα luminosity. We show the scaled SDSS galaxies in panel (2a) of Figure 12, the comparable samples of SDSS and EDisCS galaxies in panel (2b), and the corresponding distribution of Hα luminosities in panel (2c). This simple scaling brings the number of star-forming galaxies in the SDSS clusters into agreement with the EDisCS distribution. Note that because we have observed only three high-redshift clusters, we do not expect to detect high-redshift galaxies in bins where the expected counts fall below 0.33 galaxies per cluster.

While this simple model does an excellent job of reproducing the evolution of the distribution of Hα luminosities and is consistent with the evolution of the integrated Hα luminosity, we must also consider that the broad-band magnitudes of galaxies evolve. On average, galaxies have faded since $z \simeq 0.75$, and this impacts the inferred L(Hα) distribution because galaxies in the high-redshift sample may have faded below the magnitude cut
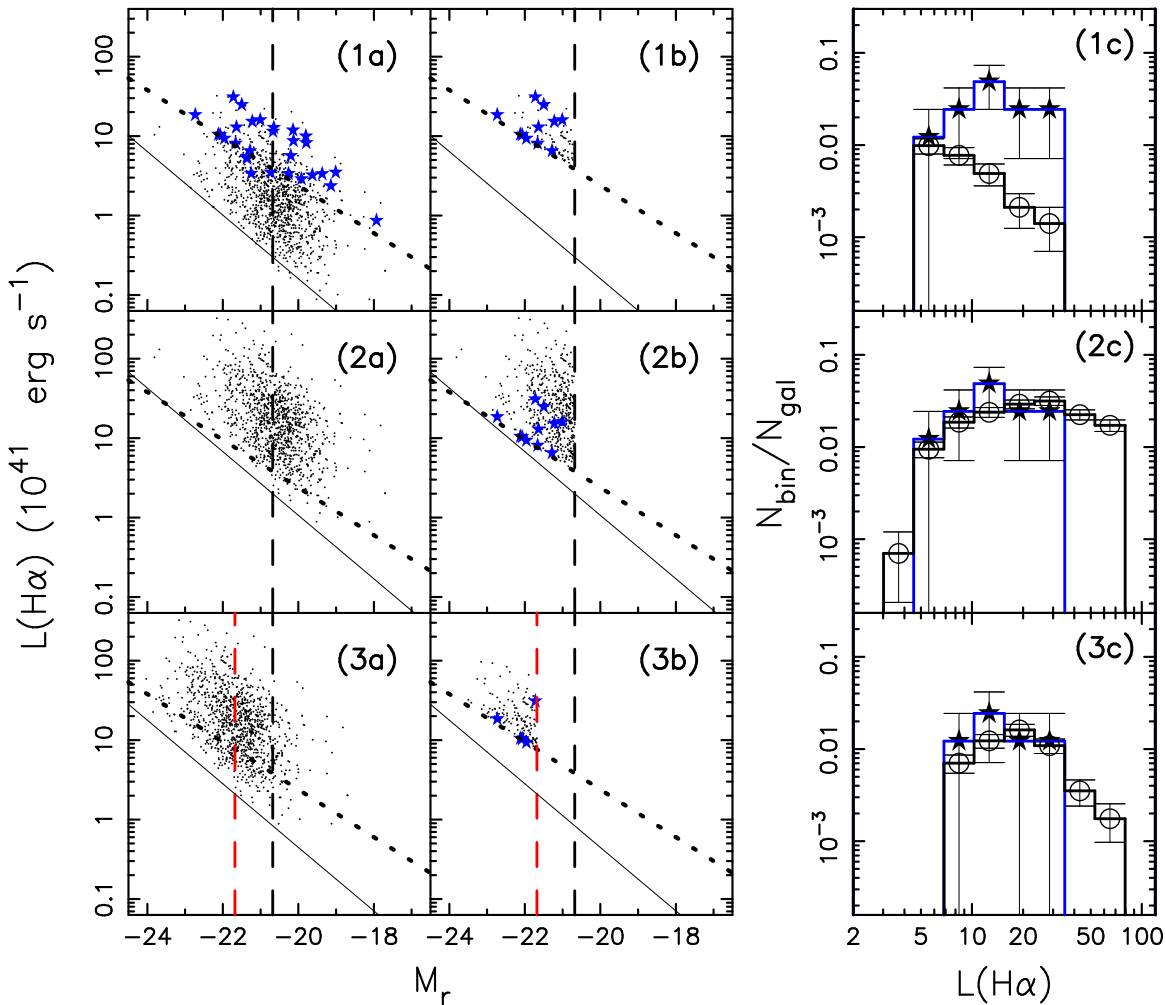
FIG. 12.— **(1a)** L(Hα) versus M_r for SDSS galaxies from 308 clusters (black dots) and $z \simeq 0.75$ galaxies (blue stars) from 3 clusters. Vertical dashed line shows spectroscopic completeness limit of SDSS. The solid line shows the EW limit of the SDSS spectra. The dotted line shows flux limit of $z \simeq 0.75$ surveys. **(1b)** Same as panel 1a but showing only those galaxies that lie above the flux and magnitude limits. **(1c)** Distribution of L(Hα) for galaxies in panel 1b. **(2a)** L(Hα) versus M_r for SDSS galaxies after L(Hα) is scaled by a factor of 10. **(2b)** Same as panel 2a but showing only those galaxies that lie above the flux and magnitude limits. **(2c)** Distribution of L(Hα) for galaxies in panel 2b. **(3a)** L(Hα) versus M_r for SDSS galaxies after L(Hα) is scaled by a factor of 3 and M_r is brightened by 1 magnitude. The red dashed line shows the magnitude of the SDSS spectroscopic completeness limit, brightened by 1 magnitude. **(3b)** Same as 3a but showing showing only those galaxies that lie above the flux and magnitude limits. **(3c)** Distribution of L(Hα) for galaxies in panel 3b.

in the low-redshift sample. We account for this in a second model by brightening each SDSS galaxy by 1 magnitude to account for fading since $z \simeq 0.75$ (e.g. Poggianti & Barbaro 1997) while simultaneously scaling the Hα luminosities of SDSS galaxies by a factor of 3. The scaled SDSS galaxies are shown in panel (3a), and the galaxies that meet the EDisCS flux cut and the SDSS magnitude cut (which is now a magnitude brighter and shown with the red dashed vertical line) are shown in panel (3b). The resulting L(Hα) distributions (shown in panel (3c)) are in reasonable agreement, although the sample of EDisCS galaxies used to derive the $z \simeq 0.75$ L(Hα) distribution is uncomfortably small.

These models show that the evolution of the star-forming cluster galaxies between $z \simeq 0.75$ and $z \simeq 0.07$ can be characterized by a fading of both the Hα and broad-band luminosities of individual galaxies. However, the two scenarios we present in Figure 12 are by no means unique, and further study is required to char-

acterize the evolution of the Hα luminosity distribution in terms of the evolution of the number, magnitudes, and star-formation rates of the star-forming galaxies. Nonetheless, these preliminary results suggest that the Hα luminosities of individual cluster galaxies have faded by a factor of up to ~ 10 since $z \simeq 0.75$. This factor of ~ 10 is an upper limit on the evolution, and it will be lower if there is evolution of galaxy magnitudes. In addition, galaxies that are presently on the red sequence may have been forming stars at $z \simeq 0.75$ (e.g. Bell et al. 2007), and this may further decrease the inferred evolution of individual Hα luminosities.

Several issues compromise our comparison of the SDSS and $z \simeq 0.75$ star-forming galaxies. The dominant limitation is the small number of high-redshift clusters. We have shown in §4 that ΣSFR exhibits large scatter as a function of cluster mass, so a more precise measure of evolution requires a much larger sample of high-redshift clusters. A second limitation is our use of Hα as a star-

formation indicator. Although relatively insensitive to dust compared with other commonly used optical indicators such as [OII] emission (e.g. Nakata et al. 2005), it is well known that a full census of star formation must account for energy re-radiated by dust (e.g. Duc et al. 2002; Coia et al. 2005; Bell et al. 2007; Bai et al. 2007). If dust obscuration is a strong function of redshift and environment, this could affect our conclusions. Furthermore, for the high-redshift clusters we are not able to quantify the AGN contamination through the Hα emission alone. AGN account for an average (median) of 23%(34%) of total Hα emission for galaxies within $0.5R_{200}$ and $\Delta v < 3\sigma$ for the SDSS clusters and 20% (average) by number. Existing studies of high-redshift clusters show low AGN fractions (e.g., Homeier et al. 2005), so AGN contamination is probably not a limiting factor in the comparison. Upcoming studies of the high-redshift clusters at X-ray and infrared wavelengths will provide some insight into the AGN fraction of the EDisCS clusters. A final caveat that may affect our findings in §4 and §5 is that the SDSS Hα luminosities are derived from aperture fluxes. Koopmann et al. (2006) find radial gradients in Hα emission that are not reflected in the radial distribution of stellar light, and this compromises the aperture correction we apply to the Hα flux. As a result, our analysis is not sensitive to processes that preferentially affect the perimeter of galaxies.

5.3. *Comparison with Field Evolution*

Field surveys show a factor of $\sim$10 decrease in ΣSFR/Mpc^3 since $z \sim 0.8$ (e.g. Tresse & Maddox 1998; Glazebrook et al. 1999; Tresse et al. 2002; Hippelein et al. 2003; Bell et al. 2007). In comparison, Figure 12 shows that we can reproduce the evolution between the star-forming galaxies in the low and high-redshift clusters by scaling the Hα luminosity of the SDSS galaxies by a factor of $\sim$ 10. This is remarkably similar to what is seen in the field, and suggests that the strong evolution observed is not driven by cluster-specific physics. However, it is important to distinguish the average star-formation rate per galaxy and the average star-formation rate of the star-forming galaxies. Recent work by Bell et al. (2007), based on the COMBO-17 photometric redshift survey, suggests that the field evolution is due in roughly equal parts to an increase in the number density of star-forming galaxies, and in the average star-formation rate per galaxy among this population. Our analysis of the Hα luminosity distribution suggests a similar division in clusters, with an increase in galaxy star-formation rates contributing about half of the factor of $\sim$ 10 observed evolution in the integrated Hα luminosity. However, we require a larger sample of high-redshift clusters, preferably with complete redshifts, and a comparable sample of high-redshift field galaxies to confirm this.

An issue that complicates the comparison in evolutionary rates between clusters and the general field is that clusters have approximately doubled their mass over the time range we are probing. However, many of the accreted galaxies may already be in the high-redshift survey volume (the $\pm 3\sigma$ velocity cut corresponds to a large volume). A careful comparison with simulations is needed to understand how infalling galaxies affect our measure of cluster star-formation properties.

5.4. *Scenarios for Declining SFRs*

Our main result is that the rate of evolution of clusters does not appear to be significantly different from that of the field. This suggests the cluster environment has not had a direct effect on galaxy star-formation rates over the past few billion years. Either the difference we observe between cluster and field populations was imprinted at high redshift, or it is driven by physics occurring on group scales (or both). Here we discuss the implications of our results on the various mechanisms frequently used to explain the decline of cluster star-formation rates. We remind the reader that our observations are restricted to relatively massive galaxies, and lower mass galaxies may behave quite differently.

If dense environments are to directly influence star-formation rates at low redshift ($z < 1$), they must presumably do so by removing gas from galaxies, since this is the dominant reservoir of baryons. Typically, discussion of such processes is divided into three types: the rapid consumption of gas, through massive starbursts; the removal of *cold* gas bound to the disk, via ram-pressure stripping (Gunn & Gott 1972) or other thermal mechanisms (Nulsen 1982); and the removal of *hot*, more loosely bound gas, through similar mechanisms (Larson et al. 1980; Kawata & Mulchaey 2007). All of these mechanisms will lead to a reduction of star formation, but they operate on different timescales and in different environments. The efficacy of ram pressure stripping depends on the velocity of the galaxy relative the ICM and the density of the ICM. Both factors reach their maximum values at the cluster center, and so ram-pressure stripping should be most effective for galaxies plunging through the middle of the cluster. One also expects that ram-pressure stripping is more effective in higher-mass clusters because they have higher-density ICMs (e.g. Mohr et al. 2000; Vikhlinin et al. 2006), and their velocity dispersions are higher. It is actually difficult to strip away *all* the cold gas in a disk, except in the centers of the most massive clusters (e.g. Quilis et al. 2000; Roediger & Brueggen 2007). The fact that we see no trends in average star-formation rate as a function of cluster mass suggests[7] that ram-pressure stripping of cold gas is not the dominant mechanism driving the evolution of star-forming cluster galaxies although it certainly occurs in some cases (Kenney et al. 2004; Koopmann et al. 2006). Instead, the decline in the star-formation rates of cluster galaxies since $z \sim 1$ must be primarily driven by physical processes that do not depend on cluster mass, at least for clusters with velocity dispersions greater than 450 km s^{-1}. A similar argument holds for the consumption of gas by starbursts, since such bursts are most easily caused by galaxy mergers which should be rare in cluster environments (but could be common in the outskirts, or in groups).

In hierarchical clustering models, clusters form in regions of high overdensity and grow through the accretion of field galaxies and groups. Most models of galaxy formation include a crude treatment of environmental

---

[7] A possible caveat is that, as noted above, Koopmann et al. (2006) show that star-formation is truncated at the outer edge of cluster spirals in Virgo, and the SDSS fiber-derived Hα fluxes are not able to detect processes that preferentially affect the outer radii of galaxies.

effects, where satellite galaxies of a halo of any mass are instantaneously stripped of their hot gas, preventing further growth of the cold gas reservoir (e.g., White & Rees 1978; Kauffmann 1995; Bower et al. 2006; Croton et al. 2006; De Lucia et al. 2006). This "starvation" mechanism (originally proposed by Larson et al. 1980) serves to shut down star formation on $\sim$1-2 Gyr timescales, starting from the instant a galaxy becomes a satellite in a larger halo. Undoubtedly this gas is easier to remove than the cold gas considered above (Kawata & Mulchaey 2007); however, it is becoming increasingly clear that the simple assumption of instant removal of gas on any satellite, regardless of halo mass, is too effective at suppressing star formation (e.g. Poggianti et al. 2006; Weinmann et al. 2006b; McCarthy et al. 2007). Our results also suggest that star-formation is not shut off immediately; rather, we see a relatively gradual fading in L(Hα) of a factor $\sim 3 - 10$ over a timespan of $\sim$7 billion years. Starvation that operates over longer timescales can also explain why field galaxies evolve at a similar rate, where the decline in field star-formation rates is due to the build-up of groups.

Another way to see this is to directly compare the amount of star formation in our clusters with predictions from the models. For this purpose, we use the publicly available Bower et al. (2006) models, based on the Millennium simulation. For each parent dark matter halo we calculate the expected value of σ and R_{200} using the same relations used here (Eqn. 2), and select galaxies based on their projected position, relative velocity (including Hubble flow and peculiar velocity components) and r-band luminosity. Using this membership criteria we compute the fraction of galaxies with Hα emission satisfying our observational criteria on flux and EW, as a function of velocity dispersion. The results are shown in Figure 13. As in the observations, there is no significant trend with velocity dispersion. However the average fraction of galaxies with Hα emission is only 10%, significantly lower than our observed value of 20% (Figure 8). This difference alone could simply be reflecting uncertainties in modeling Hα emission, which depends on the dust model, metallicity, and AGN contribution. But interestingly the average emission line fraction for the model *field* population is 36.5%, in very good agreement with our control sample value. Thus, the difference in emission-line fraction in clusters relative to the field is significantly larger in the models than in our data, and this should be robust to modeling of L(Hα) (but of course sensitive to environmental dust or metallicity effects). This lends support to our suggestion that the truncation of star formation in clusters is too severe in the current models. Note that the models assume a suppression of star formation that is not only rapid but also efficient in low mass systems, well below the mass range our cluster sample. This is because the starvation model as implemented has little dependence on the mass of the host halo, which is probably unrealistic (McCarthy et al. 2007). Recent observations suggest that groups have substantially *higher* star-formation rates than clusters (e.g. Wilman et al. 2005; Balogh et al. 2007), in contrast to these simple model predictions, and therefore these low mass systems are an important environment worthy of further study.
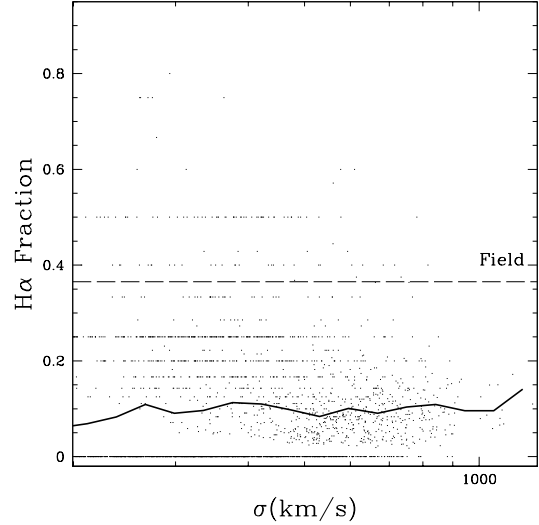

FIG. 13.— The predicted fraction of Hα-emitting galaxies versus cluster velocity dispersion for $z = 0$ clusters selected from the model of Bower et al. (2006). Each cluster is shown as an individual dot. The many clusters with no emission-line galaxies are represented with a mean of 0.05 and artificial scatter, for visualization purposes only. The galaxy magnitude limit, and Hα flux and EW limits, are the same as in our SDSS sample. The horizontal dotted line represents the average fraction among all $z = 0$ galaxies in the model (above the same magnitude limits). The thick solid line represents the average emission line fraction in bins of velocity dispersion.

6. SUMMARY & CONCLUSIONS

Using 308 dynamically relaxed, low-redshift clusters from the C4 cluster catalog, we investigate the dependence of the total stellar mass, number of star-forming galaxies, and total star-formation rate on cluster velocity dispersion. We find that the total stellar mass, the number of star-forming galaxies, and total star-formation rate scale linearly with the number of galaxies with no dependence on velocity dispersion. In other words, $\Sigma L(H\alpha)/N_{gal}$ and N_{SF}/N_{gal} are independent of velocity dispersion. We interpret this to mean that the cluster environment at low redshift does not differentially affect the star-forming properties of luminous galaxies ($M_r < -20.68$) across dense environments characterized by $\sigma > 450$ km s^{-1}.

We compare the SDSS clusters with a sample of $z \simeq 0.75$ clusters from the literature and find that the star-forming cluster population has declined significantly since $z \simeq 0.75$. Using the relationship between $\Sigma L_{H\alpha} - \sigma$ defined from the local cluster sample, we measure the mean shift in this relationship to the high-redshift cluster sample. On average (correcting for the mass growth of clusters between the two redshifts) we find that the total Hα luminosity of the high-redshift clusters is ~ 10 times greater than that of the low-redshift clusters. In more detail, we find that we are able to bring the SDSS Hα luminosity distribution into agreement with that of the high-redshift clusters by scaling the L(Hα) of individual SDSS galaxies by up to a factor of up to ~ 10, and we can reduce the required evolution in Hα luminosities to a factor of ~ 3 if we allow for fading of galaxies between $z \simeq 0.75$ and $z = 0.07$. Thus, using the SDSS clusters,

we are able to break the degeneracy between redshift and mass-evolution that limited our previous attempts to quantify the evolution of cluster star-formation properties (Finn et al. 2004, 2005).

We compare the cluster results to the evolution seen in field galaxies over a similar redshift interval. We find a factor of ∼10 decline in total star formation with decreasing redshift for the clusters as compared to a factor of ∼10 decrease for the field. Thus, we find no evidence for any differential evolution between cluster and field galaxies over this redshift range. This strengthens our conclusion that the effect of the cluster ($\sigma > 450 \mathrm{\ km\ s^{-1}}$) environment on bright, star-forming galaxies is relatively modest for $0 < z < 0.9$. In addition, the mechanism causing the decline in galaxy star-formation rates must operate over a fairly long timescale such that the star-formation rates of individual galaxies decline by an order of magnitude over ∼7 billion years, a decline timescale which is longer than galaxy evolution models commonly assume.

APPENDIX

To estimate the additional field contamination in our high redshift surveys, due to the large velocity range sampled by the narrow-band filters, we use the mock redshift survey of Yang et al. (2004). We use all halos with masses greater than 10^{14} M$_\odot$, which corresponds roughly to the mass threshold imposed by our $rm\sigma > 450\ km\ s^{-1}$ cut, and select all galaxies within $0.5 \times R_{vir}$ and $M_{B_J} < -18$. Here, Yang et al. use R_{180} to define the virialized region of each halo; this agrees to within 5% with R$_{200}$(the radial cut we have used throughout), and this slightly different radial cut does not affect the inferred contamination. We define member galaxies as those physically located within the virial radius and contamination as the number of non-members normalized by the number of observed galaxies. We calculate the contamination for late-type galaxies, which are likely to be the ones contributing to Hα emission and which also have a higher contamination rate than early-type galaxies. The simulation size is 300 h^{-1} Mpc, and the largest velocity dispersion is 2100 km/s. A $\pm 6\sigma$ velocity cut corresponds to a volume of 252 h^{-1} Mpc, so we are not limited by edge effects. We find that the contamination of late-type galaxies is 25% in a $\pm 3\sigma$ velocity cut and 31% in 6σ cut. Therefore, we correct the integrated L(Hα) of CL 1040−1155 and CL 1054−1245 by a factor of $31/25 = 0.81$ to account for additional field contamination. The Yang et al. (2004) simulation is not an ideal comparison because it is at a redshift of zero, has B-band magnitudes, and is normalized to the 2dFGRS survey. Nonetheless, it gives a useable estimate of the extra field contamination for CL 1040−1155 and CL 1054−1245.

REFERENCES

Andreon, S., Quintana, H., Tajer, M., Galaz, G., & Surdej, J. 2006, MNRAS, 365, 915

Bai, L., Marcillac, D., Rieke, G. H., Rieke, M. J., Tran, K.-V. H., Hinz, J. L., Rudnick, G., Kelly, D. M., et al. 2007, ApJ, 664, 181

Baldry, I. K., Balogh, M. L., Bower, R. G., Glazebrook, K., Nichol, R. C., Bamford, S. P., & Budavari, T. 2006, MNRAS, 373, 469

Balogh, M., Eke, V., Miller, C., Lewis, I., Bower, R., Couch, W., Nichol, R., Bland-Hawthorn, J., et al. 2004, MNRAS, 348, 1355

Balogh, M. L., Couch, W. J., Smail, I., Bower, R. G., & Glazebrook, K. 2002, MNRAS, 335, 10

Balogh, M. L. & Morris, S. L. 2000, MNRAS, 318, 703

Balogh, M. L., Morris, S. L., Yee, H. K. C., Carlberg, R. G., & Ellingson, E. 1997, ApJ, 488, L75+

Balogh, M. L., Wilman, D., Henderson, R. D. E., Bower, R. G., Gilbank, D., Whitaker, R., Morris, S. L., Hau, G., et al. 2007, MNRAS, 374, 1169

Bell, E. F., Zheng, X. Z., Papovich, C., Borch, A., Wolf, C., & Meisenheimer, K. 2007, ApJ, 663, 834

Blanton, M. R., Brinkmann, J., Csabai, I., Doi, M., Eisenstein, D., Fukugita, M., Gunn, J. E., Hogg, D. W., et al. 2003a, AJ, 125, 2348

Blanton, M. R., Eisenstein, D., Hogg, D. W., Schlegel, D. J., & Brinkmann, J. 2005, ApJ, 629, 143

Blanton, M. R., Lin, H., Lupton, R. H., Maley, F. M., Young, N., Zehavi, I., & Loveday, J. 2003b, AJ, 125, 2276

Bower, R. G., Benson, A. J., Malbon, R., Helly, J. C., Frenk, C. S., Baugh, C. M., Cole, S., & Lacey, C. G. 2006, MNRAS, 370, 645

Butcher, H. & Oemler, A. 1984, ApJ, 285, 426

Carter, B. J., Fabricant, D. G., Geller, M. J., Kurtz, M. J., & McLean, B. 2001, ApJ, 559, 606

Clowe, D., Schneider, P., Aragón-Salamanca, A., Bremer, M., De Lucia, G., Halliday, C., Jablonka, P., Milvang-Jensen, B. et al. 2006, A&A, 451, 395

Coia, D., Metcalfe, L., McBreen, B., Biviano, A., Smail, I., Altieri, B., Kneib, J.-P., McBreen, S., et al. 2005, A&A, 430, 59

Couch, W. J., Balogh, M. L., Bower, R. G., Smail, I., Glazebrook, K., & Taylor, M. 2001, ApJ, 549, 820

Croton, D. J., Springel, V., White, S. D. M., De Lucia, G., Frenk, C. S., Gao, L., Jenkins, A., Kauffmann, G., et al. 2006, MNRAS, 365, 11

De Lucia, G., Springel, V., White, S. D. M., Croton, D., & Kauffmann, G. 2006, MNRAS, 366, 499

Dressler, A., Oemler, A. J., Couch, W. J., Smail, I., Ellis, R. S., Barger, A., Butcher, H., Poggianti, B. M., et al. 1997, ApJ, 490, 577

Dressler, A., Smail, I., Poggianti, B. M., Butcher, H., Couch, W. J., Ellis, R. S., & Oemler, A. J. 1999, ApJS, 122, 51

Duc, P.-A., Poggianti, B. M., Fadda, D., Elbaz, D., Flores, H., Chanial, P., Franceschini, A., Moorwood, A., et al. 2002, A&A, 382, 60

Finn, R. A., Zaritsky, D., & McCarthy, D. W. 2004, ApJ, 604, 141

Finn, R. A., Zaritsky, D., McCarthy, D. W., Poggianti, B., Rudnick, G., Halliday, C., Milvang-Jensen, B., Pelló, R., et al. 2005, ApJ, 630, 206

Gómez, P. L., Nichol, R. C., Miller, C. J., Balogh, M. L., Goto, T., Zabludoff, A. I., Romer, A. K., Bernardi, M., et al. 2003, ApJ, 584, 210

Glazebrook, K., Blake, C., Economou, F., Lilly, S., & Colless, M. 1999, MNRAS, 306, 843

Goto, T. 2005, MNRAS, 356, L6

Gunn, J. E. & Gott, J. R. I. 1972, ApJ, 176, 1

Halliday, C., Milvang-Jensen, B., Poirier, S., Poggianti, B. M., Jablonka, P., Aragón-Salamanca, A., Saglia, R. P., De Lucia, G., et al. 2004, A&A, 427, 397

Hippelein, H., Maier, C., Meisenheimer, K., Wolf, C., Fried, J. W., von Kuhlmann, B., Kümmel, M., Phleps, S., et al. 2003, A&A, 402, 65

Homeier, N. L., Demarco, R., Rosati, P., Postman, M., Blakeslee, J. P., Bouwens, R. J., Bradley, L. D., Ford, H. C., et al. 2005, ApJ, 621, 651

Hopkins, A. M. 2004, ApJ, 615, 209

Johnson, O., Best, P., Zaritsky, D., Clowe, D., Aragón-Salamanca, A., Halliday, C., Jablonka, P., Milvang-Jensen, B. et al. 2006, MNRAS, 371, 1777

Kauffmann, G. 1995, MNRAS, 274, 161

Kauffmann, G., Heckman, T. M., Tremonti, C., Brinchmann, J., Charlot, S., White, S. D. M., Ridgway, S. E., Brinkmann, J., et al. 2003a, MNRAS, 346, 1055

Kauffmann, G., Heckman, T. M., White, S. D. M., Charlot, S., Tremonti, C., Brinchmann, J., Bruzual, G., Peng, E. W., et al. 2003b, MNRAS, 341, 33

Kauffmann, G., White, S. D. M., Heckman, T. M., Ménard, B., Brinchmann, J., Charlot, S., Tremonti, C., & Brinkmann, J. 2004, MNRAS, 353, 713

Kawata, D. & Mulchaey, J. S. 2007, ArXiv e-prints, 707

Kenney, J. D. P., van Gorkom, J. H., & Vollmer, B. 2004, AJ, 127, 3361

Kennicutt, R. C., Tamblyn, P., & Congdon, C. E. 1994, ApJ, 435, 22

Kewley, L. J., Jansen, R. A., & Geller, M. J. 2005, PASP, 117, 227

Kodama, T., Balogh, M. L., Smail, I., Bower, R. G., & Nakata, F. 2004, MNRAS, in press

Koopmann, R. A., Haynes, M. P., & Catinella, B. 2006, AJ, 131, 716

Larson, R. B., Tinsley, B. M., & Caldwell, C. N. 1980, ApJ, 237, 692

Lewis, I., Balogh, M., De Propris, R., Couch, W., Bower, R., Offer, A., Bland-Hawthorn, J., Baldry, I. K., et al. 2002, MNRAS, 334, 673

Madau, P., Pozzetti, L., & Dickinson, M. 1998, ApJ, 498, 106

McCarthy, I. G., Bower, R. G., & Balogh, M. L. 2007, MNRAS, 377, 1457

Miller, C. J., Nichol, R. C., Gómez, P. L., Hopkins, A. M., & Bernardi, M. 2003, ApJ, 597, 142

Miller, C. J., Nichol, R. C., Reichart, D., Wechsler, R. H., Evrard, A. E., Annis, J., McKay, T. A., Bahcall, N. A., et al. 2005, AJ, 130, 968

Milvang-Jensen, B., et al. 2008, A&A, submitted

Mohr, J. J., Reese, E. D., Ellingson, E., Lewis, A. D., & Evrard, A. E. 2000, ApJ, 544, 109

Moran, S. M., Ellis, R. S., Treu, T., Smith, G. P., Rich, R. M., & Smail, I. 2007, ArXiv e-prints, 707

Nakata, F., Bower, R. G., Balogh, M. L., & Wilman, D. J. 2005, MNRAS, 357, 679

Nulsen, P. E. J. 1982, MNRAS, 198, 1007

Pelló, R., Rudnick, G., Simard, L., White, S. D., Halliday, C., Milvang-Jensen, B., Poirier, S., Poggianti, B. M., et al. 2007, in prep

Poggianti, B. M. & Barbaro, G. 1997, A&A, 325, 1025

Poggianti, B. M., Smail, I., Dressler, A., Couch, W. J., Barger, A. J., Butcher, H., Ellis, R. S., & Oemler, A. J. 1999, ApJ, 518, 576

Poggianti, B. M., von der Linden, A., De Lucia, G., Desai, V., Simard, L., Halliday, C., Aragón-Salamanca, A., Bower, R., et al. 2006, ApJ, 642, 188

Popesso, P., Biviano, A., Romaniello, M., & Böhringer, H. 2007, A&A, 461, 411

Postman, M., Franx, M., Cross, N. J. G., Holden, B., Ford, H. C., Illingworth, G. D., Goto, T., Demarco, R., et al. 2005, ApJ, 623, 721

Quilis, V., Moore, B., & Bower, R. 2000, Science, 288, 1617

Rines, K. & Diaferio, A. 2006, AJ, 132, 1275

Rines, K., Geller, M. J., Kurtz, M. J., & Diaferio, A. 2005, AJ, 130, 1482

Roediger, E. & Brueggen, M. 2007, ArXiv e-prints, 707

Rudnick, G., Pello, R., Von Der Linden, A., Poggianti, B., & Milvang-Jensen, B. 2007, in prep.

Smith, G. P., Treu, T., Ellis, R. S., Moran, S. M., & Dressler, A. 2005, ApJ, 620, 78

Tresse, L. & Maddox, S. J. 1998, ApJ, 495, 691

Tresse, L., Maddox, S. J., Le Fèvre, O., & Cuby, J.-G. 2002, MNRAS, 337, 369

Vikhlinin, A., Kravtsov, A., Forman, W., Jones, C., Markevitch, M., Murray, S. S., & Van Speybroeck, L. 2006, ApJ, 640, 691

Wechsler, R. H., Bullock, J. S., Primack, J. R., Kravtsov, A. V., & Dekel, A. 2002, ApJ, 568, 52

Weinmann, S. M., van den Bosch, F. C., Yang, X., & Mo, H. J. 2006a, MNRAS, 366, 2

Weinmann, S. M., van den Bosch, F. C., Yang, X., Mo, H. J., Croton, D. J., & Moore, B. 2006b, MNRAS, 372, 1161

White, S. D., Clowe, D., Simard, L., Rudnick, G., De Lucia, G., Aragón-Salamanca, A., Bender, R., Best, P., et al. 2005, A&A, 444, 365

White, S. D. M. & Rees, M. J. 1978, MNRAS, 183, 341

Wilman, D. J., Balogh, M. L., Bower, R. G., Mulchaey, J. S., Oemler, A., Carlberg, R. G., Eke, V. R., Lewis, I., et al. 2005, MNRAS, 358, 88

Yang, X., Mo, H. J., Jing, Y. P., van den Bosch, F. C., & Chu, Y. 2004, MNRAS, 350, 1153

York, D. G., Adelman, J., Anderson, J. E., Anderson, S. F., Annis, J., Bahcall, N. A., Bakken, J. A., Barkhouser, R., et al. 2000, AJ, 120, 1579